X-645-73-243

PREPRINT

HIGH-LATITUDE DAYSIDE ELECTRIC FIELD AND PARTICLE MEASUREMENTS

NELSON C. MAYNARD
ALAN D. JOHNSTONE

AUGUST 1973

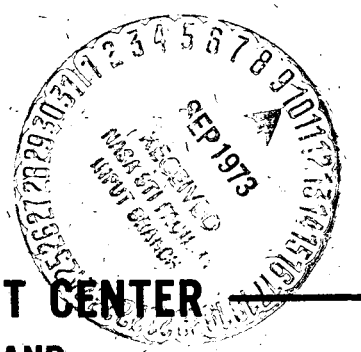

GSFC — GODDARD SPACE FLIGHT CENTER —
GREENBELT, MARYLAND

High-Latitude Dayside Electric Field and Particle Measurements

Nelson C. Maynard
Alan D. Johnstone*

Goddard Space Flight Center
Greenbelt, Maryland 20771

August 1973

*NAS-NRC Fellow
Present Address: Mullard Space Science Laboratory
University College, London
Dorking, Surrey, England

Abstract

Two rockets carrying electric field and low energy particle instrumentation were launched near noon at 80° magnetic latitude. One flight encountered polar cap conditions only while the other traversed part of the polar cusp. Although weak particle precipitation was measured on both flights, bursts of intense magnetosheath-type electron fluxes were detected on the latter. Strong electric fields such as would result from anti-sunward convection were observed during both flights. The measurements are compared with results obtained by other types of spacecraft and interpreted in the light of those data.

Introduction

It was first suggested by Chapman and Ferraro (1931) that two neutral points would be formed on the surface of the current sheet between the solar plasma cloud and the earth's magnetic field and that plasma could enter what we now know as the magnetosphere through these points. The concept was developed when the existence of the solar wind and a permanent magnetosphere became known as it was realized that the neutral points allowed a continuous leakage of plasma from the solar wind into the magnetosphere. Calculations of the leakage rate have been made by Spreiter and Summers (1967) and Willis (1969) who obtained a value of 5×10^{24} protons/sec. Recent observations using particle detectors on satellites (Heikkila and Winningham 1971, Frank 1971, Frank and Ackerson 1971, Russell, et al., 1971) have confirmed the existence of the neutral points and detected the leakage of particles at various altitudes above the earth from 1000 kms to many earth radii showing that the spectrum of the particles is very similar to that of magnetosheath particles. Hoffman (1972) completed a detailed survey of a "soft zone" of particle precipitation at low altitudes which coincides on the dayside with this neutral point or "polar cusp" region. His excellent time resolution showed considerable temporal-spatial structure leading him to call it the zone of "bursts".

The observed particle fluxes have emphasized the concept of a neutral line (Piddington, 1965) as opposed to a point. Frank (1971) hypothesised that the polar cusp is spatially connected to the distant plasma sheet in the magnetotail with the cusp field lines being convected around the flank of the magnetopause. Winningham (1971) has put the longitudinal width of the cusp as from 0800 to 1600 (MLT magnetic local time). The width in

latitude according to Heikkila and Winningham (1971) is 2 to 5 degrees and to Frank (1971) is 0.2 to 4 degrees. The cusp moves toward the equator during times of magnetic activity as the front side of the magnetosphere is compressed. In quiet periods it is centered near 80° invariant latitude.

The particle spectra observed in the polar cusp have been very soft, corresponding closely to that observed in the magnetosheath. Electron spectra generally peak around 100 volts while proton energies are somewhat higher, with the peak energy nearer 1 kev (Winningham, 1972; Frank, 1971).

Electric fields at high latitudes during daylight hours have been measured by observations of barium releases (Wescott et al., 1970; Heppner et al. 1971a and b) which require twilight, and the satellite traversals of OGO-6 (Heppner, 1972a) and INJUN-5 (Cauffman and Gurnett, 1971). The polar cap electric fields are relatively quiet compared to auroral zone measurements and are typically 10 to 30 mV/m dawn-dusk resulting in anti-sunward convection. Heppner (1972) using OGO-6 data found the polar cusp region electric fields to be extremely variable with large variations ($\Delta E \sim$ 30-100 mV/m) occurring in short spatial or temporal intervals (see his Figure 8). A satellite passes through structure in this region at about 8 km/sec. Gurnett (1972) shows a reversal of the field at the trapping boundary and an eastward electric field (anti-sunward convection) in the polar cusp region. Broadband VLF hiss seen in this region is believed to be generated by low energy polar cusp electrons (Gurnett and Frank, 1972).

We report here joint particle and electric field measurements in the polar cusp region made from two rockets launched during periods with different levels of worldwide magnetic activity.

Rocket Performance

The Fox Main DEW (Distant Early Warning) Line Station at Hall Beach, N.W.T., Canada was chosen as the launch site because of its proximity to the polar cusp region (68.757°N, 81.224°W geographic; 79.728°N, 23.816°W geomagnetic). Two Nike-Tomahawk rockets (18.126 and 18.127) were launched in a northwesterly direction reaching an apogee of approximately 315 kms. Since both flights took place in daylight, ground magnetic records were used to choose the launch time. On March 15, 1971 at 11 hr 19m local time (17:19Z) 18.126 was launched. The magnetic horizontal disturbance vector was close to the direction of the normal polar cap disturbance but was abnormally large. 18.127 was launched on March 18, 1971, at 11.00 LT (17:00Z) into a disturbance whose horizontal direction was considerably different from that of a normal polar cap disturbance. The ground observations are discussed in more detail in a separate section.

No radar or other tracking data were available at this temporary launch site. The trajectory was constructed by calculating a theoretical trajectory, including coriolis forces, using nominal values for launch direction and motor performance. Parameters were then adjusted using total elapsed time, passage through the lower E region (as determined by the electric field and particle data) and approximate peak times to best fit the data. The result is a vertical velocity profile that is reasonably accurate and a horizontal velocity that is set only by nominal trajectory data. Apogee was estimated as 315 km for 18.126 and 318 km for 18.127.

The attitude of the rocket was measured using two sun sensors for a solar reference and two fluxgate magnetometers for a magnetic field reference. A complete attitude solution was obtained once per roll. A summary of the attitude data for the two flights is given in Table 1. The accuracy of the solution is estimated as $\pm 2^{\circ}$.

Instrumentation

Both rockets carried identical instrumentation consisting of a single axis electric field experiment and five low energy particle detectors.

The electric field was measured by the double floating probe technique (Aggson, 1969) using cylindrical, motor extended antennas 6.09 m. long as the sensors. The probes were insulated from the plasma with a Kapton coating over the inner 3.05 m. making the distance between the mid-points of the active element 9.3 m. The floating potential of each probe was measured by a voltage follower, having an input impedance greater than $10^{11}\Omega$ to prevent "voltmeter errors", and then differentially subtracted. The resultant signal, proportional to the vector sum $\vec{E} + \vec{V} \times \vec{B}$, was monitored using two gain ranges for the DC and a four channel spectrometer covering the AC spectrum from 0.03 to 100 kHz. The antennas were not deployed until atmospheric drag had decreased to a safe level; hence deployment was not completed until the rocket had passed 170 km. altitude.

The particle detectors were channel electron multipliers with cylindrical energy analyzers. The four electron detectors were identical in configuration. The fifth detector, used to measure protons, had a channel multiplier with a larger aperture. Two of the electron energy analyzers had fixed voltages applied to the plates which centered their passband near 700 eV. The other two, and the proton detector had a stepping voltage that scanned the spectrum in eight steps, equally spaced logarithmically from about 300 eV to 3000 eV. Each step was held for 50 m sec. giving a complete scan in 0.4 sec.

Two of the electron detectors, one fixed, one stepping, were mounted to look at 20° to the spin axis of the rocket. The other two and the proton

detector were mounted at 60° to the spin axis on the opposite side of the rocket as illustrated in Figure 1. The geometric factor (calculated theoretically (Johnstone 1972) of the electron detectors was 1.2×10^{-5} E (eV) cm^2 ster eV and of the proton detector 9.3×10^{-5} E (eV) cm^2 ster eV. The energy bandwidth of all five was 19%. The pulses from the detectors were counted in logarithmic accumulators which were read out simultaneously and reset every 25 m secs.

Electric Field Data

The electric field data were scaled each spin cycle to determine the amplitude and phase of the signal containing the sum of the ambient electric field and the induced $\vec{v} \times \vec{B}$ electric in the spin plane. Contact potential errors, appearing as a constant offset of the sinusoidal signal, are easily removed. The attitude solution was used to transform $\vec{v} \times \vec{B}$ obtained from the trajectory calculations into the rocket system where it was vectorially subtracted from the total measured field. The resultant $\vec{E}$ was transformed back to the earth-fixed topographical system using the attitude solution. There is an estimated error in these processes of ±2% in the larger component and ±5% in the smaller component arising from inaccuracies in the attitude solution. There is an additional error of ±3 mv/m from the data handling and other physical considerations. Errors in the trajectory also can have an effect on the total error. A 20% variation in the horizontal velocity made a maximum shift of ±2° in the direction of the resultant field (±3% of the smaller component).

Figure 2 shows the data from 18.126. At the top of the figure is the total measured field (spin plane) and the total $\vec{v} \times \vec{B}$ (all 3 axes). The topographic X and Y components after the vector subtraction are shown

below. Note that the gross amplitude and direction remain relatively constant over the whole flight. The small periodic changes in azimuth (116 sec period) are precession effects from errors in the attitude solution. Small amplitude fluctuations (5 to 7 mV/m) are prevalent in both components throughout the flight. The average magnitude of 30-40 mV/m is similar to that of previous measurements in the polar cap (Heppner 1972a; Heppner et al., 1971; Cauffman and Gurnett 1971) but on the high side of the average, perhaps an indication of the high overall disturbance level or as suggested by Gurnett's (1972) data that the region of stronger convection extends a short way into the cap region. The field direction is 20° - 30° sunward of the easterly direction expected from anti-sunward convection over the polar cap.

In Figure 3 the data from 18.127 is displayed in a similar way. The vertical scale is compressed compared with Figure 2. Several differences are obvious. The magnitude early in the flight is much larger ~ 100 mV/m but gradually decreases to 40 mV/m at the end of the flight. The fluctuations also decrease in magnitude and at the end of the flight are much smaller than for 18.126. The direction is very close to 90° (due East) throughout the flight corresponding to anti-sunward convection. Some of the fluctuations, near 0230 and 0450 are associated with strong fluxes of low energy electrons (described below). Both magnitude and direction changes are prevalent at these times.

Figure 4 shows data from the four channel spectrometer for both flights. Each of the broadband filters covers about a decade in frequency range. 18.126 is characterized by a lack of activity in the three upper channels. The variations in the 30-100 H_z channel show some orientation dependence

and are similar to low frequency variational signals observed on satellites (Maynard and Heppner 1970). The low frequency noise observed in to 100 to 120 km region is similar to that reported by Holtet et al., (1971). The noise detected by 18.127 was entirely different in character. It is most intense in the top two channels reaching saturation for much of the time over the first half of the flight in the 10 - 100 kH_z channel. This indicates auroral hiss which has been shown by Hoffman and Laaspere (1972) to be present in regions where low energy particle precipitation exists. The hiss had dropped to a low level by the time the last particle bursts were seen (around 4.45 to 5.35 min.) and remained low over the rest of the flight. It is also interesting to note the anti-correlation of the noise in the two lower frequency channels with that in the upper channels. In a recent paper Gurnett and Frank (1972) have found noise near 100 Hz in in the polar cusp region that they have compared to lion's roar, a phenomena found in the transition region by Smith et al., (1969). This would show up in both lower channels and offers an alternative to the ELF noise and irregularities as an explanation of the data.

Particle Data

In Figure 5 the 0.8 second averages of the counting rate of the detector with fixed energy (720 eV) and at pitch angles between 0° and 40° are shown for both flights. During the flight of 18.126 there was weak precipitation throughout. The detector on 18.127 also found this background of weak precipitation but also saw short bursts of very much more intense precipitation. Burst structures are evident near 120 sec. and 290 sec., corresponding to areas of variations in the electric fields (See Figure 3). In the analysis below we have concentrated on the bursts

occurring between T+285 sec. and T+310 sec. in the 18.127 data when the rocket was close to its apogee of 319 km. At this altitude the atmospheric effects, which are shown to be important, are minimized.

The observed electrons are seen to have a strong pitch angle dependence which is apparent from the ratio of the counting rates of the detectors at different pitch angles and in the spin modulation of the counting rate of each detector. The detectors at 20° to the spin axis are mounted on the opposite side of the rocket from those at 60° (see Figure 1). Then, since the spin axis of the rocket is about 16° from the magnetic field and the coning angle is small, when one detector is at 4° pitch angle the other is at 76° and one half spin later one is at 36° while the other is at 44°. In the latter case both detectors are looking very nearly at the same pitch angle and should observe nearly the same intensity, if there are no azimuthal variations. This gives an inflight inter-calibration between each pair of detectors. The ratio of the counting rates of the two detectors, at pitch angles α_1, α_2 we call the anisotropy A (α_1, α_2). The ratio has been formed for each point in the period T+283 to T+315 in the flight of 18.127 and averaged in 2° ranges of the pitch angle of the 60° detector. The results are independent of time and average intensity but depend quite strongly on particle energy. The greatest intensities are observed for particles with small pitch angles. These facts suggest that the anisotropy may be the result of atmospheric absorption alone. To test this the following model of the atmospheric interaction was used. The electrons are supposed to lose energy continuously, without straggling or scattering. The model is most likely to be valid near the top of the atmosphere before many scattering collisions have occurred. In Table 2 some relevant values

taken from Berger et al., (1970) have been listed. The particles can reach the rocket after only a small number of scattering collisions although the lower energy particles have lost a significant proportion (20%) of their energy. Then the intensity observed at a depth h pitch angle α and energy E is that corresponding to a primary energy of E^1 where

$$E^1 = E + h \sec \alpha \left(\frac{dE}{dh}\right).$$

It is shown below that the energy spectrum has the form $Ae^{-E/Eo}$. Then

$$\ell n\, A(\alpha_1, \alpha_2) = \frac{h}{E_o} \frac{dE}{dh} (\sec \alpha_2 - \sec \alpha_1) \quad (\alpha_1 > \alpha_2).$$

dE/dh is a function of the particle's current energy but its variation during the energy loss above the rocket has been ignored. In Figure 6, ℓn A is plotted against (sec α_2 - sec α_1) and a least squares fit line drawn through the points. The intercept of this line with the A-axis is a measure of the difference between the two detectors. For both energies apparently the 20° detector is about twice as sensitive as the 60° detector. This probably is incorrect and a result of the inaccuracy of the theory. The slope of the curve m gives

$$m = (h/Eo)(dE/dh)$$

Some values of (dE/dh) calculated from the Bethe formula are tabulated by Berger et al., (1970) for electrons E > 200 eV. They are listed in Table 2 for the examples in Figure 7. Taking E_o = 110 eV we obtain

$$n = 5.2 \times 10^{-7} \text{ gm cm}^{-2} \quad (300 \text{ eV})$$

$$= 4.9 \times 10^{-7} \text{ gm cm}^{-2} \quad (720 \text{ eV})$$

The agreement is remarkable and indicates that even if the theory is inaccurate in detail the relative amounts of anisotropy at the two energies is in proportion to their stopping powers and hence is likely to be of atmospheric origin. Using extreme assumptions about the relation of the lines in Figure 6 to the points makes relatively little effect on the calculated depth which remains in the range $4 - 6 \times 10^{-7}$ gm cm^{-2}. This is because the anisotropy is an exponential function of the depth so that a small change in depth gives big change in the anisotropy. The high fluxes are only observed over a small range of altitudes relative to a scale height near apogee so that an altitude variation cannot be found in the data. The variation of neutral atmospheric parameters is listed by Anderson and Francis (1966) for various local times and levels of solar activity. Calculating from values listed in their tables, the extremes range of values of the depth at 318 kms is from 1.9×10^{-8} gm cm^{-2} to 5.6×10^{-7} gm cm^{-2}. The derived value is within this range but at the high end; rather higher than one would expect for the polar regions at the equinox at a fairly low level of solar activity. The increase could be caused by atmospheric heating by the particles being measured. The main result of this analysis is that the anisotropy could be entirely the result of an atmospheric interaction. The primary pitch angle distribution of the electrons could be isotropic between 0° and 90°.

Electron Spectrum

All the spectral measurements are taken from the stepped energy detector at 20° to the spin axis. It covers a pitch angle range of 0° - 40°

which leads to an anisotropy at 300 eV of $A(0^\circ, 40^\circ) = 1.3$ if caused by the atmospheric interaction. This is much smaller than the time variation in the intensity and has been ignored. At these small pitch angles the modification of the particle spectrum by atmospheric energy loss is minimized. To this end all the spectra are taken during the time when the rockets were within 10 kms of their apogee. Each has been averaged over several cycles of the energy range to improve the accuracy. The intensity changes considerably in this time. To remove the effect of the time variations the counting rate of the 720 eV detector was averaged in the same way and the ratio (swept/720 eV fixed) counting rates was taken. This procedure is only valid if the spectral shape does not change with intensity or time. No evidence can be found for such effects or for effects of velocity dispersion. The level of the spectrum is fixed by the average level of the 720 eV electrons over the time interval. The electron intensities have been converted to phase space densities by

$$D(m^{-6}\ sec^{3}) = \frac{I(cm^{2}ster^{-1}eV^{-1}\ sec^{-1})}{E(eV) \times 10^{18} \times 6.18}$$

No allowance has been made for the efficiency of the channel multiplier detectors being less than 100% or varying with energy. Most reported measurements show that it is near 100% with only small variations in this energy range (Paschmann et al, 1970). The spectra are plotted in Figure 7. The three 'burst' spectra are taken during the events between T + 285 secs. and T + 310 secs. in the flight of 18.127. The two background spectra are averaged over 60 sweeps near apogee.

The following features are noted:

1. All the spectra are linear on a logarithmic plot with approximately the same slope. The exponents in this power-law approximation range from -3.7 to -4.5. Although the fit is not as good, a Maxwellian velocity distribution has been fitted to the spectra to facilitate comparisons with other observations. The resultant temperatures range from 1 to 2 x 10^6 °K.
2. Despite the different geophysical circumstances of the two flights the spectra of the background precipitation are very similar in level and slope.

No velocity dispersion is observed during time variations in the measured fluxes, although the analysis is difficult when one detector steps in energy. During an extremely intense burst at T +290 secs. on 18.127, when the 720 eV intensity reached 8.5 x 10^6 electrons cm^{-2} $ster^{-1}$ eV^{-1} sec^{-1} the dispersion between 300 eV and 720 eV is estimated to be less than 24 msecs. This places the source of the modulation, if temporal, within 700 km of the rocket. Clearly, such structure could not have originated near the magnetopause but must either be a result of the particles' passage through the ionosphere, or be spatial structure in the beam.

Proton fluxes were observed throughout both flights with no significant time variations in either flight. It is impossible to obtain reliable spectra from the measurements because of the effects of charge-exchange and energy loss in the atmosphere. There are much higher fluxes in the upper half of the energy range 1 keV < E < 3 keV) than in the electron measurements.

Ground Magnetic Data

Data from thirteen ground magnetometers were examined to determine the magnetic conditions at the time of both flights. The period from 0200 UT

to 0500 UT at all stations and from 0100 UT to 0600 UT at many stations on March 21st, 1971, was exceptionally quiet with all three components of the magnetic field being nearly constant. This period was chosen to give the baseline for determining the disturbance vectors. Both horizontal and vertical disturbance vectors were measured at the beginning of each flight and are shown in Figure 8 in a magnetic latitude - magnetic local time coordinate system. The launch site at Fox Main is plotted with a circle around it and also with the typical electric field vector measured in flight.

During the flight of 18.126, Fox Main was in a region with a large amplitude disturbance (192γ for ΔH at Fox Main) having a relatively uniform direction over much of the polar cap. This region extended as far south as Baker Lake (73.8° geomagnetic latitude). The direction was parallel to the usual polar cap disturbance with the vector directed toward 1500 MLT (Silsbee and Vestine, 1942). The vertical disturbance was near zero. The electric field vector was 20 to 30° toward 1800 LT (or more easterly) relative to $\vec{\Delta H}$.

The disturbance at Resolute, Thule and Alert had the same orientation during the flight of 18.127, but the magnitude was smaller than in 18.126. The orientation of the vector at Godhaven, Fox Main and Baker Lake was quite different. The magnitude was much larger than the auroral zone stations at Churchill and Great Whale but in the same general direction. The vertical disturbance at Fox Main was slightly negative. Thus, in this case, the rocket was not in the polar cap region; and, from the particle observations, we conclude that it was in the region of the polar cusp. The typical electric field vector here was toward 1800 MLT or due east (anti-sunward convection direction).

Figure 9 shows the variation of the planetary magnetic index Kp during the period of both flights. For the 12 hours before and during the period of the flight the average Kp for 18.126 was 4- while for 18.127 it was 1+. The dependence of the position of the polar cusp with Kp has been established by Hoffman (1972) and Heikkila and Winningham (1971). Hoffman showed that an increase of Kp from 1 to 3 created a southward movement of the boundary of 3 to 4°. This is consistent with the interpretation that 18.126 was in the polar cap while 18.127 penetrated the cusp.

Discussion

In order to compare the particle measurements with other relevant measurements we have plotted Figure 10. All the reported data have been fitted to a simple Maxwellian distribution and a density and temperature derived. Each measurement is than plotted in n/T space. Some caution is necessary when interpreting this diagram because of the assumptions made in deriving n and T. In general measurements made at energies between 200 eV and 700 eV have been used. Exceptions are those of Hoffman (1972) (700 eV to 2300 eV) and Ogilvie et al, (1971) (under 200 eV). The derived temperatures are higher at higher energies, as is the case for the spectra in Figure 7. The magnetosheath densities and temperatures are very variable and very few measurements have been reported. Of those used here, the measurements of Ogilvie et al, (1971) were made down-stream from the neutral points near the dawn magnetopause and those reported by Russell et al, (1971) were made during a very disturbed period. The following points can be made: (a) The cusp temperatures are slightly higher on average. This may be a result of a small amount of stochastic acceleration giving increased densities in the high energy tail of the distribution, (b) Peak densities observed at low altitude approach those in the magnetosheath, (c) The

densities reported by Frank (1971) and Winningham (1972) are much lower than those reported by other workers. The reason for this is not obvious but may be an instrumental effect. The spectrometers of Frank and Heikkila and Winningham (1971) had much wider energy passbands (exceeding 60%) than most of the other instruments. Also, since they were stepping through the energy range, their time resolution was not as good. Hence the weaker fluxes may be the result of spectral and spatial averaging over the very variable fluxes we report here. A satellite, moving more than 10 times as fast as the rocket through the structure detected during the flight of 18.127 would be unable to make a measurement of the spectrum if the basic time resolution is not much better than 1 second. Some of the disagreement over the latitude width of the polar cusp region (Winningham 1972) may be the result of differing sensitivities. It is interesting to observe that the densities reported by Winningham and Frank are close to the background levels measured in the two rocket flights.

Figure 11 shows the electric field and particle data from 18.127 on an expanded time scale for the precipitation event between 287 and 310 sec. The best resolution of the electric field data is one point per spin since one spin cycle best defines both components. Finer structure can be seen but not resolved into magnitudes and directions. The particle data are 100 msec. totals of the fixed energy detector at small pitch angles. The electric field in the vicinity of the strongest fluxes is at times very slightly depressed. Since the ionosphere is sunlit, and the low energy particles do not penetrate deeply into the E region, there are unlikely to be changes in the conductivity significant enough to modify the electric

field by loading the source. Peaks in magnitude and changes in direction of the field are associated with some of the "edges" in the particle structure. This can possibly be explained by the charge density in the spatial structure of the precipitating beam. The density of electrons measured by our detector was 0.8 cm^{-3} which is more than enough to cause the observed effects in a beam of reasonable thickness. The negative charge may be neutralized to some extent by unmeasured positive particles although the proton detector measured no fluctuations correlated with the bursts of electrons. Note that in addition precipitation peak occurred near 330 sec (05:30) without significant electric field effects.

The measured flux of electrons corresponds to a current density of approximately 1.3×10^{-10} amps cm^{-2}. In a companion flight using a vector magnetometer, Ledley and Farthing (private communication) found narrow intense changes in the magnetic field which they suggest are caused by field-aligned currents. They do not have enough information to define the direction of these currents. Their horizontal scale size was about 1 km, similar to the horizontal scale size of the precipitated electron bursts. If the current is the result of the electron precipitation then it is directed upwards, away from the Earth, whereas the model of Heppner et al. (1971) requires a net current towards the Earth to explain ground magnetic measurements. Not enough is known about upward electron fluxes and downward proton fluxes in the neighborhood of the rocket to be sure the net current is downward.

The easterly direction of the electric field corresponding to anti-sunward convection is consistent with a model such as Dungey's (1961) where merging occurs at the boundary of the magnetosphere and those field lines just to the north are open to the magnetosheath plasma. Gurnett and Frank (1972) show westward and eastward convection components in this area; however in all cases there is an anti-sunward component in their result in the cusp region (their instrument detects only one component of the perpendicular electric field). The variability of the OGO-6 measurements in this region (Heppner, 1972a) indicates that there may exist either a very irregular structure to the cusp or that the fields are greatly influenced by local inhomogeneities. All measurements in this area have found large magnitude fields.

The interplanetary magnetic field measured by IMP-6 at the time of 18.127 was toward the sun and westward ($\phi \sim 310^{\circ}$) with a θ_{SE} (north-south) direction of + 20 to 30°. This interplanetary field would fit best the situation for Heppner's (1972b) type A pattern or uniform convection across the polar cap. This also is consistent with our easterly directed electric field. 18.126 was launched at the time the interplanetary field switched north after about 4 hours of southward directed field. The ϕ direction had been toward the sun for over an hour. Heppner's (1972b) convection patterns would predict either a flat pattern or one with larger convection toward evening as typical for this case. The electric field was basically easterly, but with a southerly component pushing the convection toward the evening side. From the interplanetary magnetic field direction for 18.127, Wilhjelm and Friis-Christensen (1971) and Jørgensen, et al., (1972) would predict a westward Hall current in the polar cusp region. While this current would

be consistent with the ground magnetic disturbance at Fox Main (see Figure 8), it is inconsistent with the observed electric field for either a Hall or Pedersen current in that direction.

Magnetic field lines in and around the cusp are presumably those involved in merging at the boundary or those having recently merged and are being swept back into the tail. Thus, the velocity of the field lines near the boundary in the cusp should be close to that of the bulk plasma in the adjacent magnetosheath. Using the model of Dryer and Faye-Petersen (1966), this is estimated as 0.5 v_∞ (where v_∞ is the solar wind velocity-typically about 400 km/sec.), which results in a 200 km/sec. velocity. Assuming field lines can not pile up, the separation at any point in the cusp between two field lines is given by

$$\frac{d}{v} = \text{const.}$$

where d is the separation and v is the velocity. The electric field that we found to be 50 to 100 mv/m in the cusp corresponds to a convection velocity of 1 to 2 km/sec. This value is in agreement with the measurements of Heppner (1972) and Gurnett and Frank (1973). Thus, the width at the orifice should be 100 to 200 times the width in the ionosphere or the angular width should be 10 to 20 times the ionospheric angular width assuming the boundary to be at 10 R_e. Lower ionospheric electric fields increase the ratio. Figure 12 shows two field lines, 0.1° apart in the ionosphere, calculated from the model of Sugiura and Poros (1973). The model, based on fitting the OGO's 3 and 5 $\Delta\vec{B}$ data, predicts the separation ratio of 100 in distance, although it places the cusp at a higher latitude(83°). Frank (1971) has put the typical width in distant regions to be the order

of 1 R_e or 6° in latitude. Thus, the region directly open to the magnetosheath in the above discussion is quite narrow at ionospheric altitudes with a scale size nearer that of the bursts than that of the overall region. The large variations in electric field seen by Heppner (1972a) and the multiplicity of bursts in the particle data would suggest that many such small openings may exist in a turbulent pattern giving rise to the observed wider soft zone.

Conclusions

1. 18.126, launched during a magnetically disturbed period made measurements in the polar cap: 18.127, under quieter magnetic conditions, traversed part of the polar cusp, passing into the polar cap during the last part of the flight.

2. The intense electron fluxes detected in the polar cusp had temperatures between 1 and 2 x 10^6 °K similar to magnetosheath electrons. Peak densities approached those measured in the magnetosheath indicating that magnetosheath electrons have direct access to the polar ionosphere through the polar cusp.

3. The observed anisotropy could have been caused entirely by the atmospheric interaction.

4. Electron and proton precipitation was observed at a low level during both flights. The spectrum of this background electron precipitation had the same slope as the intense bursts but the intensities were orders of magnitude lower. No proton bursts were observed.

5. VLF hiss was only observed during the flight of 18.127 and while it was not directly correlated with the measurements of intense electron precipitation, it was found in the same general region.

6. Fluctuations in the electric field at the 'edge' of intense electron precipitation may be caused by the charge density in the beam.

7. Large amplitude easterly electric fields (anti-sunward convection) were observed during both flights although in the polar cusp the fields were larger and more variable. Polar cap electric fields near the cusp were found to be larger than the typical values observed over the whole polar cap by satellites.

8. The electric field and particle data argue for a cusp structure that is very variable with small regions of direct magnetosheath access within the overall region.

Acknowledgements

The authors are indebted to Drs. J. P. Heppner, R. A. Hoffman, M. Sugiura and J. L. Burch for helpful discussions in obtaining and interpreting these results. We wish to thank Dr. D. H. Fairfield for the use of the IMP-6 data. We are grateful for the hospitality and support of the DEW Line personnel, and the technical support of Thiokol Chemical Corporation and GSFC personnel of both the Sounding Rocket Division and Laboratory for Space Physics in performing these launches. The hard work of S. Tammara Rao in the data analysis of the particle results is gratefully acknowledged. The work was carried out while ADJ held an NAS/NRC Resident Research Associateship at the Goddard Space Flight Center.

TABLE 1

ROCKET	SPIN PERIOD secs	CONING PERIOD secs	α degrees	β degrees
18.126	0.814	116	21.5°	14°
18.127	0.844	124	16°	3°

Attitude data for both flights. α is the angle between the coning axis and the magnetic field. β is the coning half-angle.

TABLE 2

	300 eV	720 eV
Energy loss by veritcal electron	61 eV	39.5 eV
No. of scattering collisions	2.5	1.1
Median scattering angle per collision	23°	16°
Energy loss rate eV/gm cm^{-2}	1.82×10^8	1.26×10^8

Some values from Berger et al., (1970) relevant to the atmospheric interaction of the precipitating electrons. They refer to a depth of 3.2×10^{-7} gm cm^{-2}.

/

References

Aggson, T. L., Probe measurements of electric fields in space, Atmospheric Emissions, ed. by B. M. McCormac and A. Omholt, Van Norstrand Reinhold, New York, 305 1969.

Anderson, A. D., and W. E. Francis, The variation of the neutral atmospheric density with local time and solar activity from 100 to 10000 keV J. Atmos. Sci., 23 110, 1966.

Berger, M. J., S. M. Seltzer, and K. Maeda, Energy deposition by auroral electrons in the atmosphere, J. Atmos. Terr. Phys., 132, 1015, 1970.

Burch, J. L., Low energy electron fluxes at latitudes above the auroral zone, J. Geophys. Res., 73, 3585, 1968.

Cauffman, D. P., and D. A. Gurnett, Double probe measurements of D.C. electric fields with the INJUN-5 satellite, J. Geophys. Res., 6014, 1971.

Chapman, S. and V.C.A. Ferraro, A new theory of magnetic storms, Terrest. Magnetism Atmospheric Elec. 36, 77, 1931.

Dryer, M., and R. Faye-Petersen, Magnetogasdynamic boundary condition for a self-consistent solution to the closed magnetopause, AIAA Journal, 4, 246, 1966.

Dungey, J. W., Interplanetary magnetic field and the auroral zone, Phys. Rev. Letters, 6, 47, 1961.

Frank, L. A., Plasma in the earth's polar magnetosphere, J. Geophys. Res., 76, 5202, 1971.

Frank, L. A., and K. L. Akerson, Observations of charged-particle precipitations into the auroral oval, J. Geophys. Res., 76, 3612, 1971.

Gurnett, D. A., Electric field and plasma observations in the magnetosphere, in Critical Problems of Magnetospheric Physics, ed. by E. R. Dyer, IUCSTP Secretariat, Washington, 123, 1972

Gurnett, D. A., and L. A. Frank, ELF noise bands associated with auroral electron precipitations, J. Geophys. Res., 77, 3411, 1972.

Gurnett, D. A., and L. A. Frank, Observed relationships between electric fields and auroral particle precipitation, J. Geophys. Res., 78, 145, 1973.

Heikkila, W. J. and J. D. Winningham, Penetration of magnetosheath plasma to low altitudes through the dayside magnetospheric cusps, J. Geophys. Res., 76, 883, 1971.

Heppner, J. P., Electric field variations during substorms: OGO-6 measurements, Planet. Space. Sci., 20, 1475, 1972a.

Heppner, J. P., Polar cap electric field distributions related to the interplanetary magnetic field direction, J. Geophys. Res., 77, 4877, 1972b.

Heppner, J. P., J. D. Stolarik, and E. M. Wescott, Electric field measurements and the identification of currents causing magnetic disturbances in the polar cap, J. Geophys. Res., 76, 6028, 1971a.

Heppner, J. P., J. D. Stolarik, and E. M. Wescott, Field-aligned continuity of Hall currents, electrojets and other consequences of density gradients in the auroral ionosphere, in The Radiating Atmosphere, ed. by B. M. McCormac, D. Reidel, Dordrecht, Netherlands, 1971b.

Hoffman, R. A., Properties of low energy particle impacts in the polar domain in the dawn and dayside hours, in Magnetosphere-Ionosphere Interactions, ed. by K. Folkestad, Universitetsforlaget, Oslo, 117, 1972.

Hoffman, R. A., and T. Laaspere, A comparison of VLF auroral hiss with precipitating low-energy electrons using simultaneous data from two OGO-4 experiments, J. Geophys. Res., 77, 640, 1972.

Holtet, J., A. Egeland, and N. C. Maynard, Rocket, ground and satellite measurements of ELF emissions during a PCA, in The Radiating Atmosphere, ed. by B. M. McCormac, D. Reidel, Dordrecht, Holland, 345, 1971.

Johnstone, A. D., The geometric factor of a cylindrical plate electrostatic analyser, Rev. Sci, Inst., 43, 1030, 1972.

Jørgensen, T. S., E. Friis-Christensen, and J. Wilhjelm, Interplanetary magnetic field direction and high latitude ionospheric currents, J. Geophys. Res., 77, 1976, 1972.

Maynard, N. C., and J. P. Heppner, Variations in electric fields from polar orbiting satellites, in Particles and Fields in the Magnetosphere, ed. by B. M. McCormac, D. Reidel, Dordrecht, Holland, 247, 1970.

Montgomery, M. D., J. R. Asbridge, and S. J. Bain, Vela 4 plasma observations near the earth's bow shock, J. Geophys. Res., 75, 1217, 1970.

Ogilvie, K. W., J. D. Scudder, and M. Sugiura, Magnetic field and electron observations near the dawn magnetopause, J. Geophys. Res., 76, 3574, 1971.

Paschmann, G., E. G. Shelley, R. D. Sharp, and L. F. Smith, Absolute efficiency measurements for channel electron multipliers using a unique electron source, Rev. Sci. Inst., 41, 1706, 1970.

Piddington, J. H., The magnetosphere and its environs, Planet. Space Sci., 13, 363, 1965.

Russell, C. T., C. R. Chappell, M. D. Montgomery, M. Neugebauer, and F. C. Scarf, OGO-5 observations of the polar cusp on Nov. 1, 1968, J. Geophys. Res., 76, 6743, 1971.

Silsbee, H. C., and E. H. Vestine, Geomagnetic bays, their frequency and current system, Terrest. Magnetism Atmospheric Elec., 47, 195, 1942.

Smith, E. J., R. E. Holtzer, and C. T. Russell, Magnetic emissions in the magnetosheath at frequencies near 100 Hz, J. Geophys. Res., 74, 3027, 1969.

Spreiter, J. R., and A. L. Summers, On conditions near the neutral points on the magnetospheric boundary, Planet. Space Sci., 15, 787, 1967.

Sugiura, M., and D. J. Poros, A magnetic field model incorporating the OGO-3 and 5 magnetic field observations, Planet. Space Science., in press, 1973.

Wescott, E. M., J. D. Stolarik, and J. P. Heppner, Auroral and polar cap electric fields from barium releases, in Particles and Fields in the Magnetosphere, ed. by B. M. McCormac, D. Reidel, Dordrecht, Holland, 229, 1970.

Wilhjelm, J., and E. Friis-Christensen, Electric fields and high latitude zonal currents induced by merging of field lines, Danish Meteorological Institute Report, R-31, Charlottenlund, Denmark, 1971.

Willis, D. M., The influx of charged particles at the magnetic cusps on the boundary of the magnetosphere, Planet. Space Sci., 17, 339, 1969.

Winningham, J. D., Characteristics of magnetosheath plasma observed at low altitudes in the dayside magnetospheric cusps, in Earth's Magnetospheric Processes, ed. by B. M. McCormac, D. Reidel, Dordrecht, Holland, 1972.

Figures

Figure 1 - A sketch of the layout of the particle detectors in the rocket. The angles of acceptance of the detectors in the plane containing the spin axis is shown. The magnetic field direction lay on or within the cone indicated during the flight.

Figure 2 - The electric field observed on 18.126. At the top is the total measured $\vec{E} + \vec{v} \times \vec{B}$ in the spin plane compared to the total $\vec{v} \times \vec{B}$. At the bottom are the north-south and east-west components (north and east are positive) and the azimuth of the resultant electric field vector from north.

Figure 3 - The electric field observed on 18.127. The format is the same as Figure 2.

Figure 4 - Results of the 4-channel spectrometers for measuring AC electric fields for both 18.126 and 18.127.

Figure 5 - The variation of intensity of precipitating 720 eV electrons during both flights. In 18.126 the intensity is averaged over 0.76 secs; in 18.127, over 0.78 secs.

Figure 6 - The anisotropy of the electron intensity at two energies. The plot is explained in the text. The lines are least-squares fit to the sets of points.

Figure 7 - Spectra from the intense bursts between T + 286 and T + 310 secs. on 18.127 and the background precipitation at apogee on both flights.

Figure 8 - Magnetic disturbance vectors for 13 polar stations at the beginning of each flight. The Fox Main station (launch site) is circled and the typical electric field vector as measured during the flight is also plotted at Fox Main. Scale lengths for both plots are on the 18.127 plot.

Figure 9 - The planetary magnetic index Kp for six days during which both rockets were fired.

Figure 10 - A summary of published measurements of electrons in the magnetosheath and polar cusp. Points with rings refer to magnetosheath measurements. References are:

B - Burch 1968

F - Frank 1971

H - Hoffman 1971

M - Montgomery et al, 1970

O - Ogilvie et al, 1971

R - Russell et al, 1971

W - Winningham 1972

1, 2, 3 bursts spectra in Figure 7

4, 5 background spectra in Figure 7

Figure 11 - A comparison of particle data and electric field measurements during the intense bursts observed by 18.127.

Figure 12 - Two field lines at the polar cusp as defined by the model of Sugiura and Poros (1973). The field lines are for 82.9 and 83.0° and illustrate the difference in the separation near the boundary compared with the separation at ionospheric altitudes.

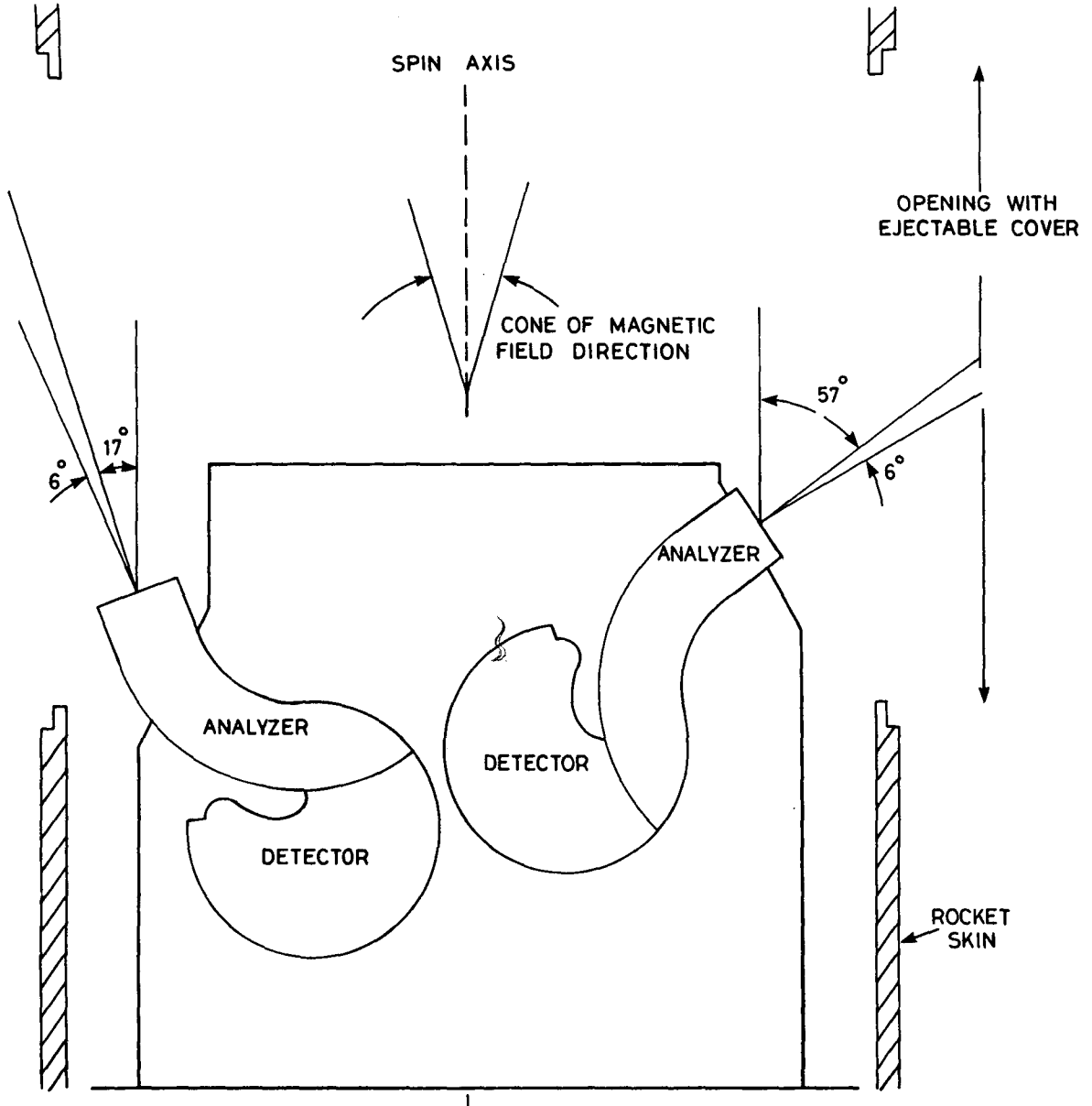
SPIN AXIS
OPENING WITH
EJECTABLE COVER
CONE OF MAGNETIC
FIELD DIRECTION
57°
17°
6°
6°
ANALYZER
ANALYZER
DETECTOR
DETECTOR
ROCKET
SKIN

Figure 1

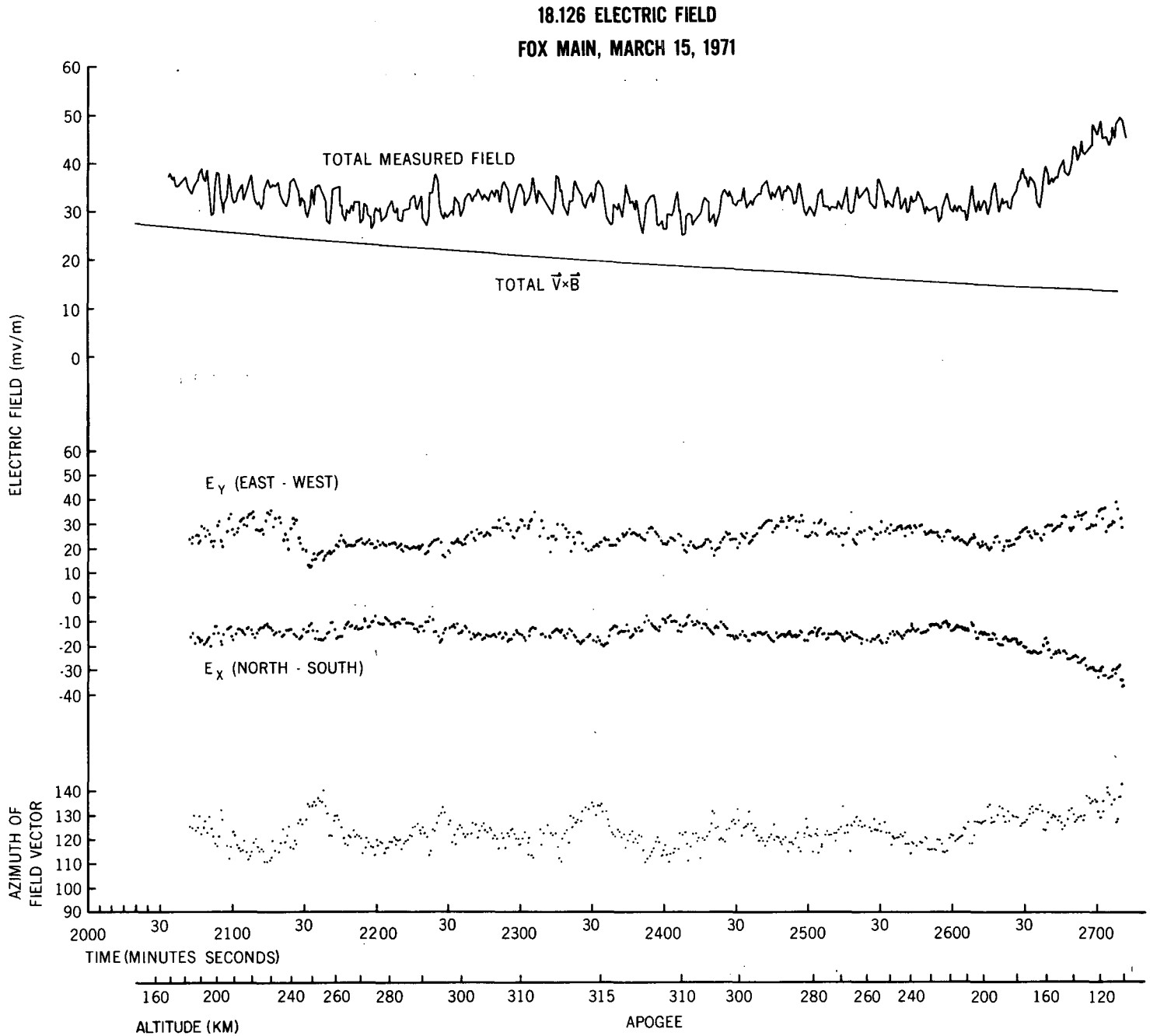
18.126 ELECTRIC FIELD
FOX MAIN, MARCH 15, 1971
ELECTRIC FIELD (mv/m)
TOTAL MEASURED FIELD
TOTAL $\vec{V}\times\vec{B}$
E_Y (EAST - WEST)
E_X (NORTH - SOUTH)
AZIMUTH OF FIELD VECTOR
TIME (MINUTES SECONDS)
ALTITUDE (KM)
APOGEE

Figure 2

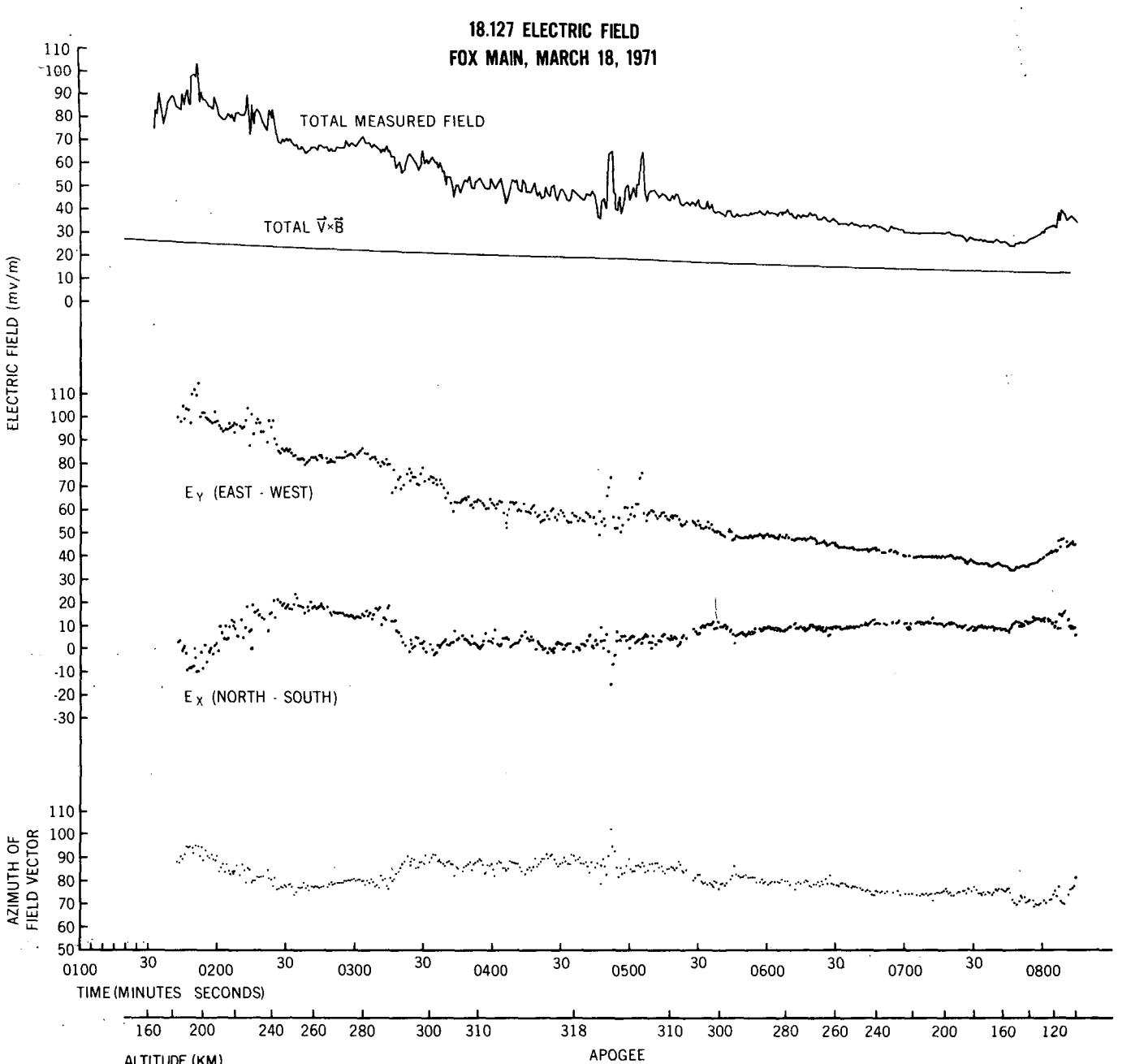
18.127 ELECTRIC FIELD
FOX MAIN, MARCH 18, 1971
TOTAL MEASURED FIELD
TOTAL $\vec{V}\times\vec{B}$
ELECTRIC FIELD (mv/m)
E_Y (EAST - WEST)
E_X (NORTH - SOUTH)
AZIMUTH OF FIELD VECTOR
TIME (MINUTES SECONDS)
0100 30 0200 30 0300 30 0400 30 0500 30 0600 30 0700 30 0800
ALTITUDE (KM)
160 200 240 260 280 300 310 318 310 300 280 260 240 200 160 120
APOGEE

Figure 3

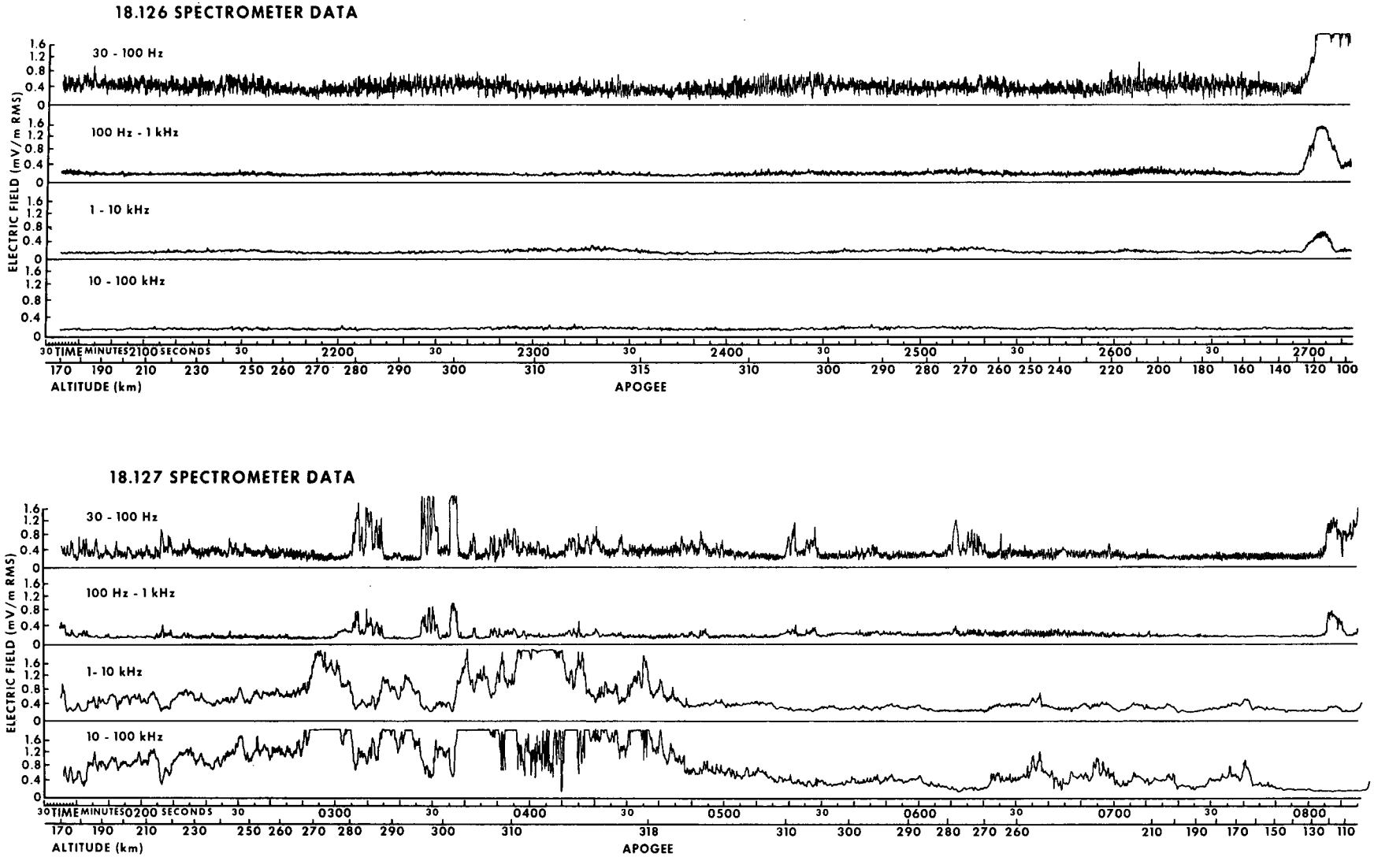
18.126 SPECTROMETER DATA
30 - 100 Hz
100 Hz - 1 kHz
1 - 10 kHz
10 - 100 kHz
ELECTRIC FIELD (mV/m RMS)
TIME MINUTES 2100 SECONDS 30 2200 30 2300 30 2400 30 2500 30 2600 30 2700
ALTITUDE (km)
APOGEE
18.127 SPECTROMETER DATA
30 - 100 Hz
100 Hz - 1 kHz
1- 10 kHz
10 - 100 kHz
ELECTRIC FIELD (mV/m RMS)
TIME MINUTES 0200 SECONDS 30 0300 30 0400 30 0500 30 0600 30 0700 30 0800
ALTITUDE (km)
APOGEE

Figure 4

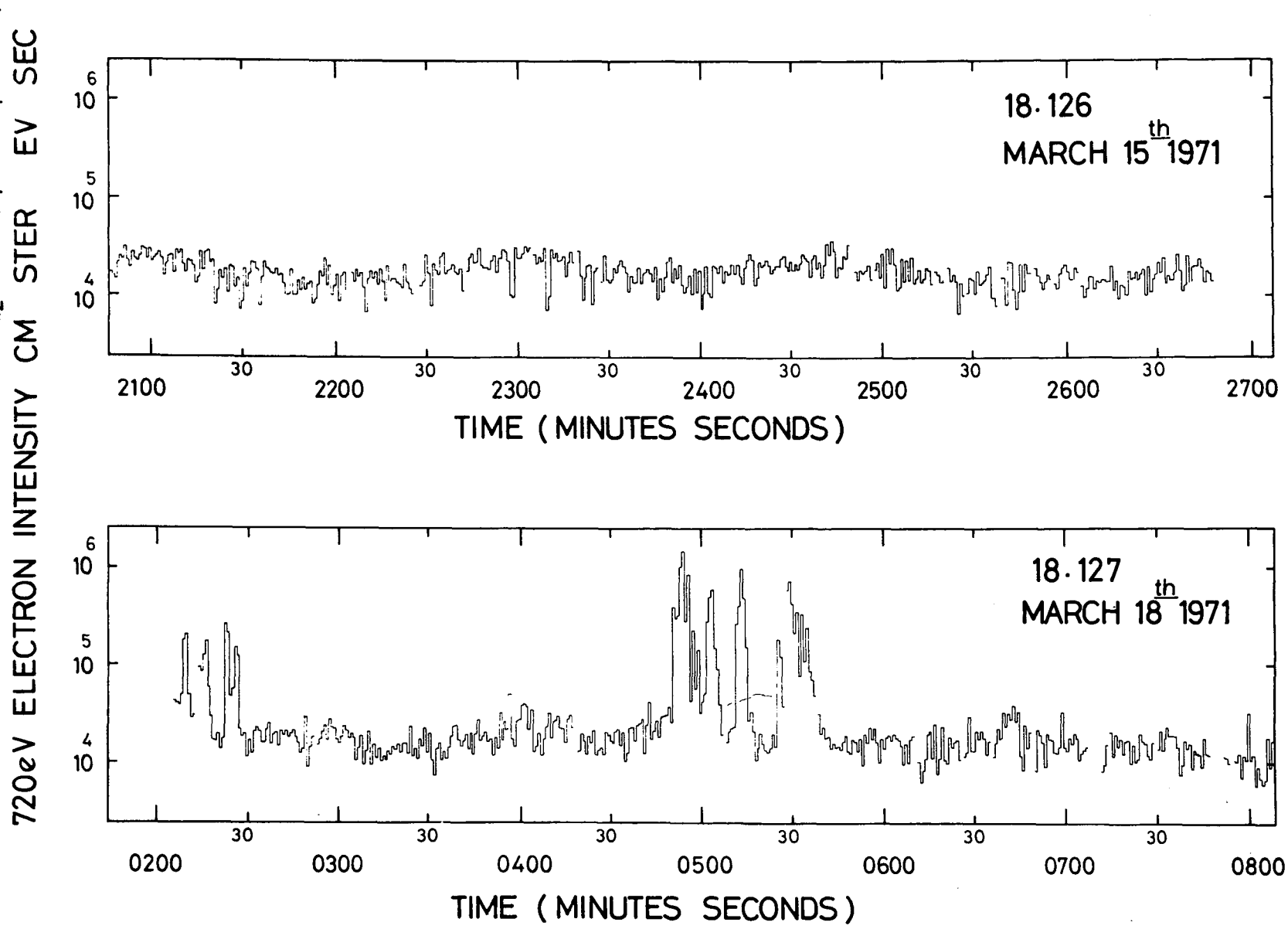
720eV ELECTRON INTENSITY CM^{-2} STER^{-1} EV^{-1} SEC^{-1}
10^6
10^5
10^4
18·126
MARCH 15th 1971
2100
30
2200
30
2300
30
2400
30
2500
30
2600
30
2700
TIME (MINUTES SECONDS)
10^6
10^5
10^4
18·127
MARCH 18th 1971
30
0200
30
0300
30
0400
30
0500
30
0600
30
0700
0800
TIME (MINUTES SECONDS)

Figure 5

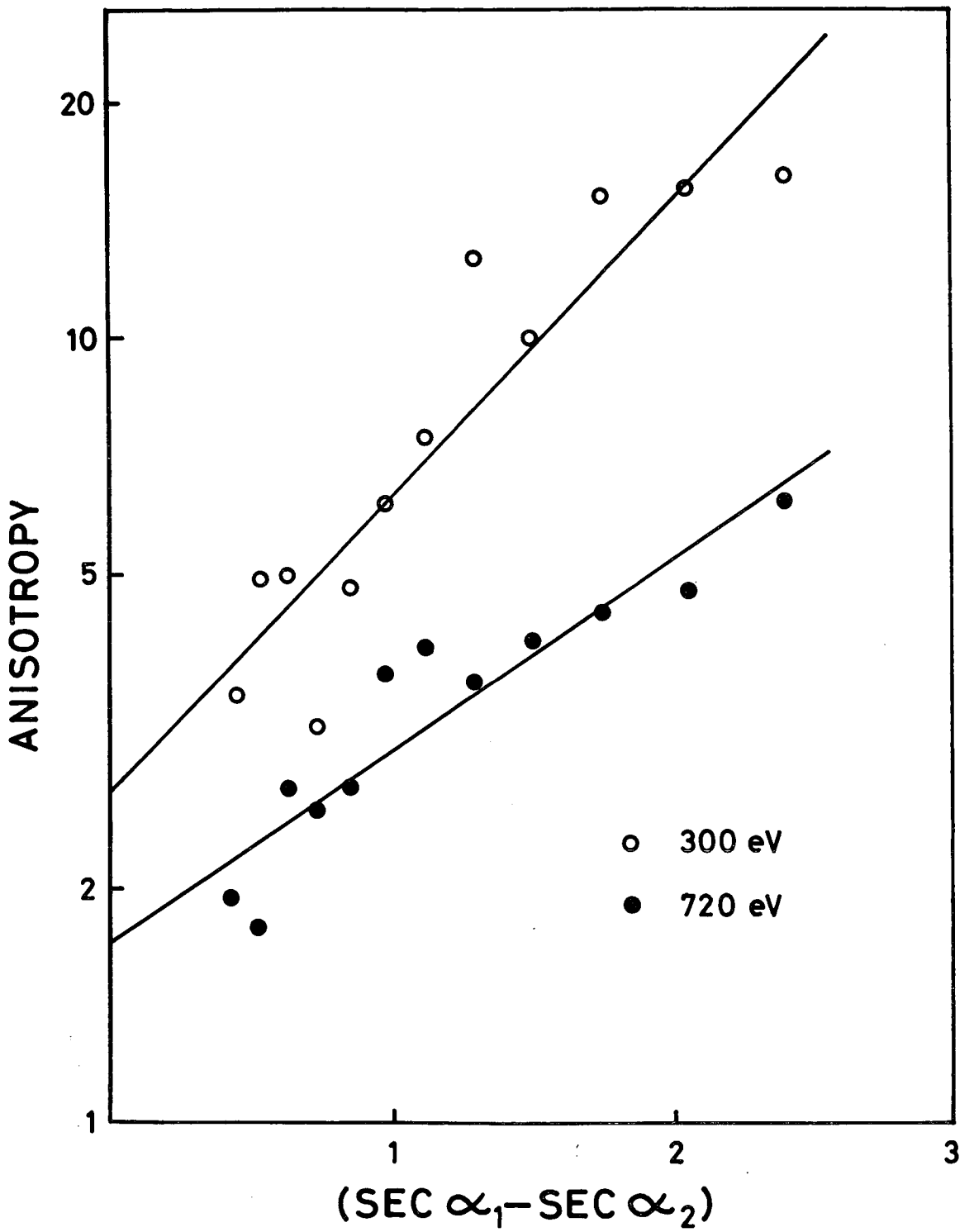

Figure 6

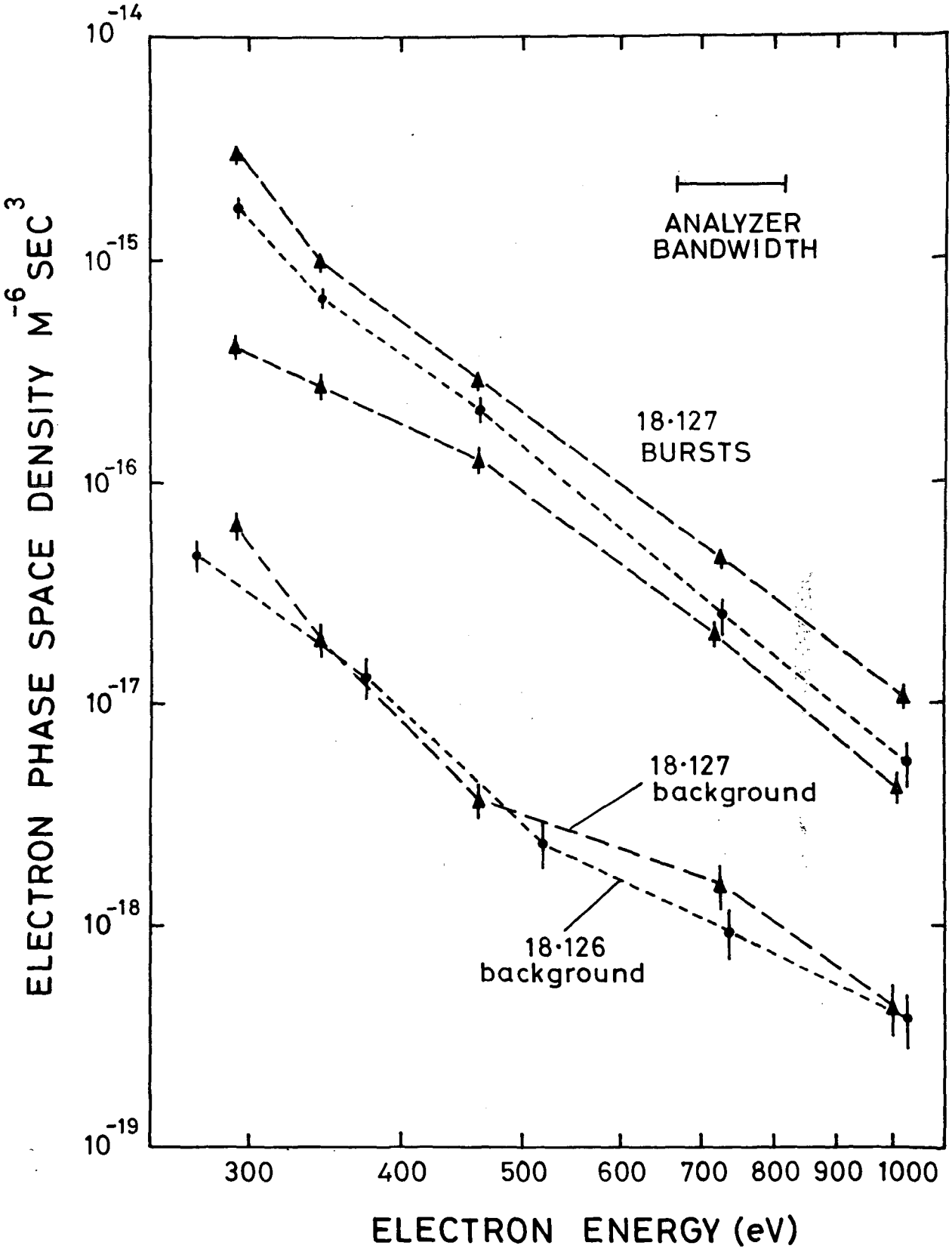
ELECTRON PHASE SPACE DENSITY M^{-6} SEC^{3}
10^{-14}
10^{-15}
10^{-16}
10^{-17}
10^{-18}
10^{-19}
ANALYZER BANDWIDTH
18·127 BURSTS
18·127 background
18·126 background
300
400
500
600
700
800
900
1000
ELECTRON ENERGY (eV)

Figure 7

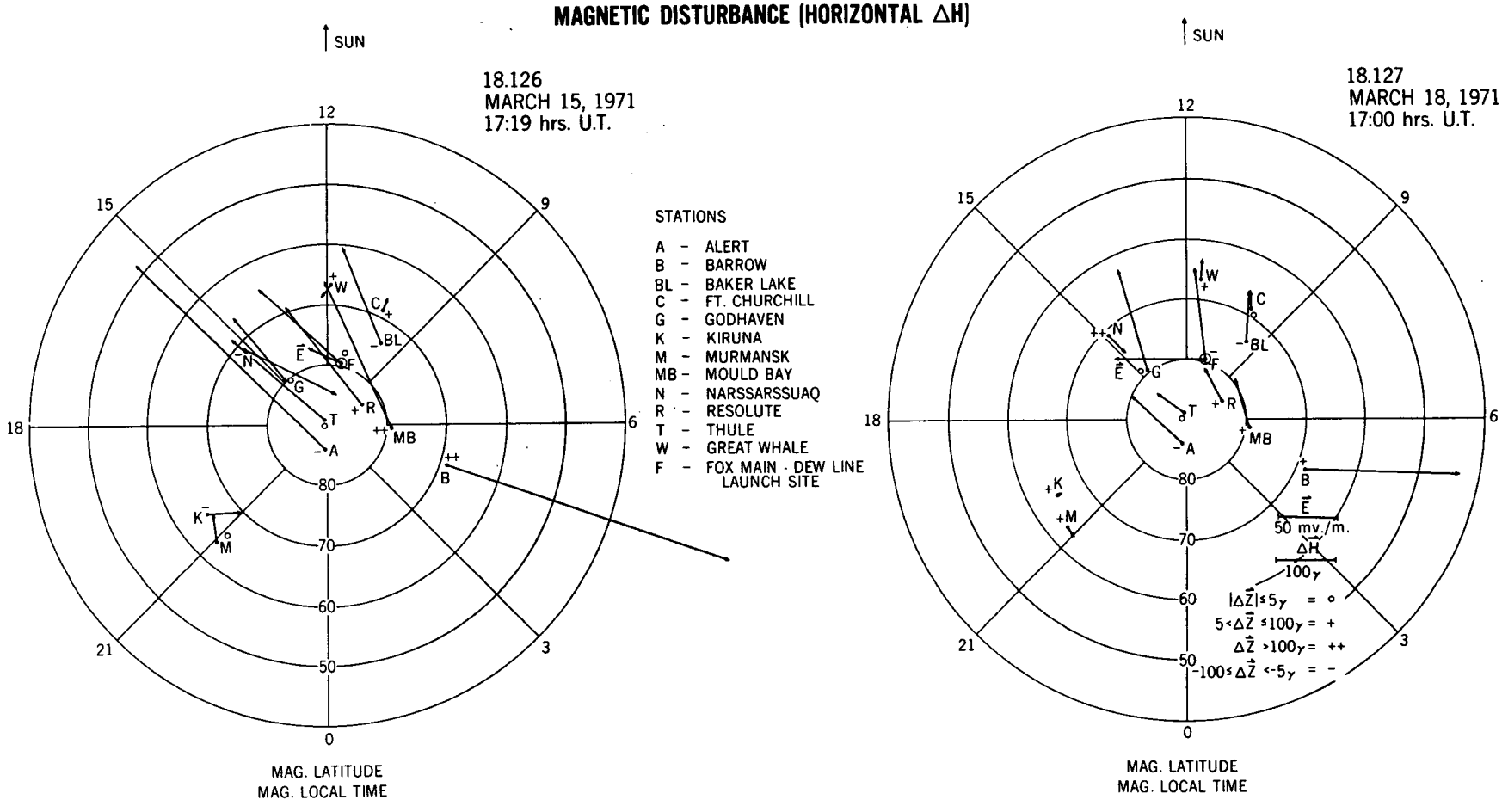
MAGNETIC DISTURBANCE (HORIZONTAL ΔH)
SUN
18.126
MARCH 15, 1971
17:19 hrs. U.T.
STATIONS
A - ALERT
B - BARROW
BL - BAKER LAKE
C - FT. CHURCHILL
G - GODHAVEN
K - KIRUNA
M - MURMANSK
MB - MOULD BAY
N - NARSSARSSUAQ
R - RESOLUTE
T - THULE
W - GREAT WHALE
F - FOX MAIN - DEW LINE LAUNCH SITE
MAG. LATITUDE
MAG. LOCAL TIME
SUN
18.127
MARCH 18, 1971
17:00 hrs. U.T.
50 mv./m.
100γ
|ΔZ| ≤ 5γ = o
5 < ΔZ ≤ 100γ = +
ΔZ > 100γ = ++
-100 ≤ ΔZ < -5γ = -
MAG. LATITUDE
MAG. LOCAL TIME

Figure 8

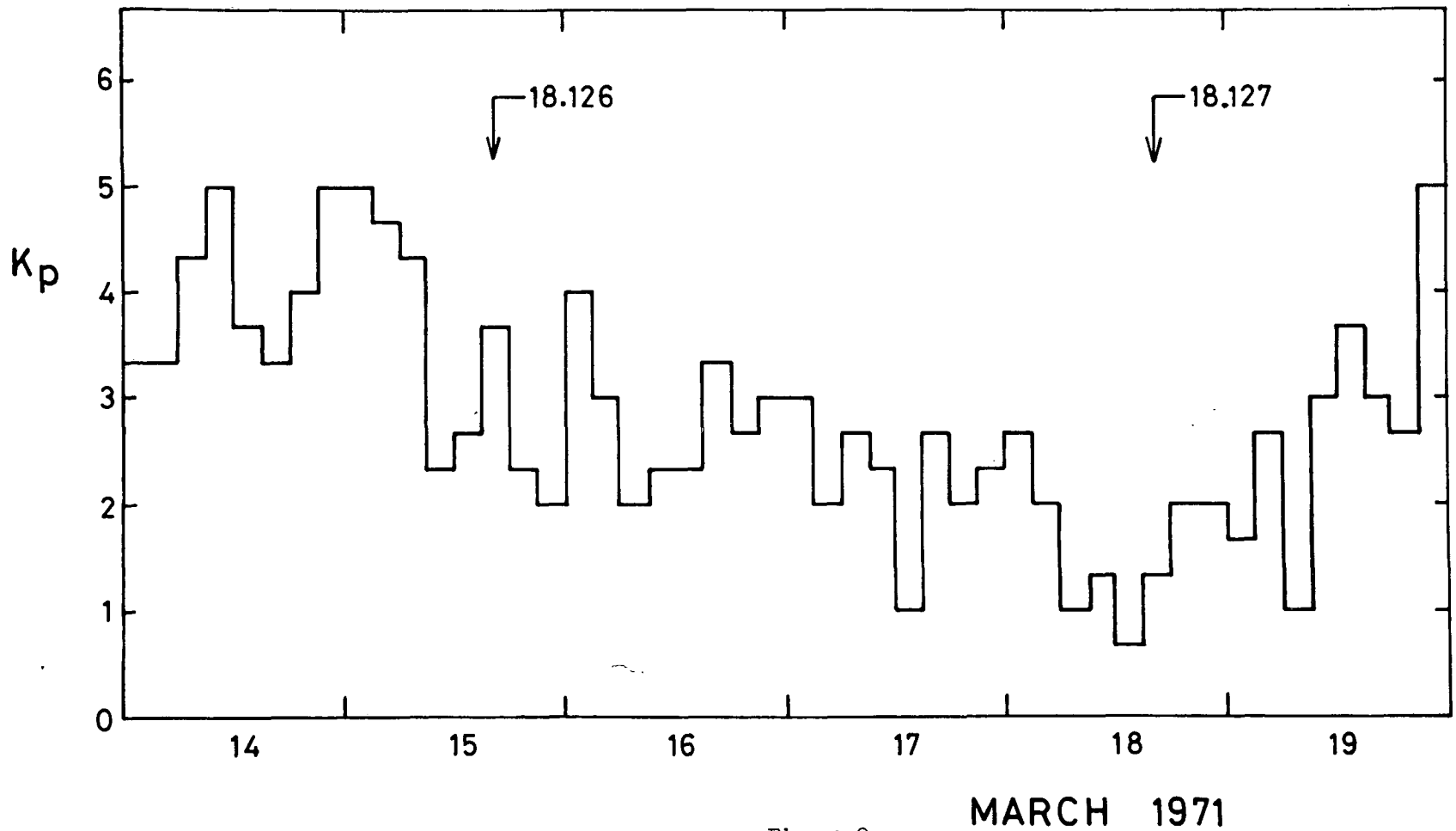

Figure 9

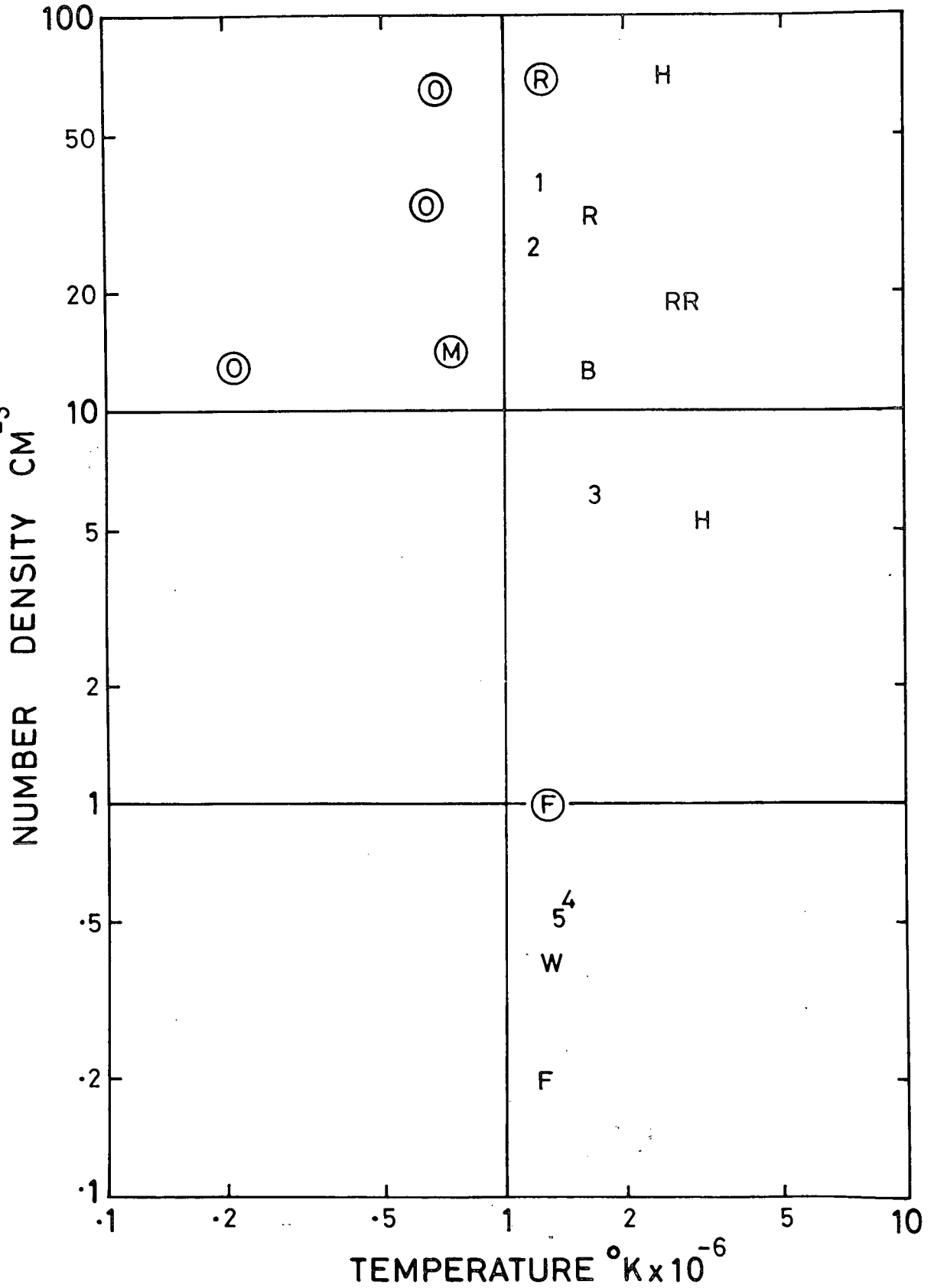
100
50
20
10
5
2
1
·5
·2
·1
NUMBER DENSITY CM^{-3}
·1
·2
·5
1
2
5
10
TEMPERATURE °K x 10^{-6}
O
O
O
M
R
H
1
R
2
RR
B
3
H
F
5
4
W
F

Figure 10

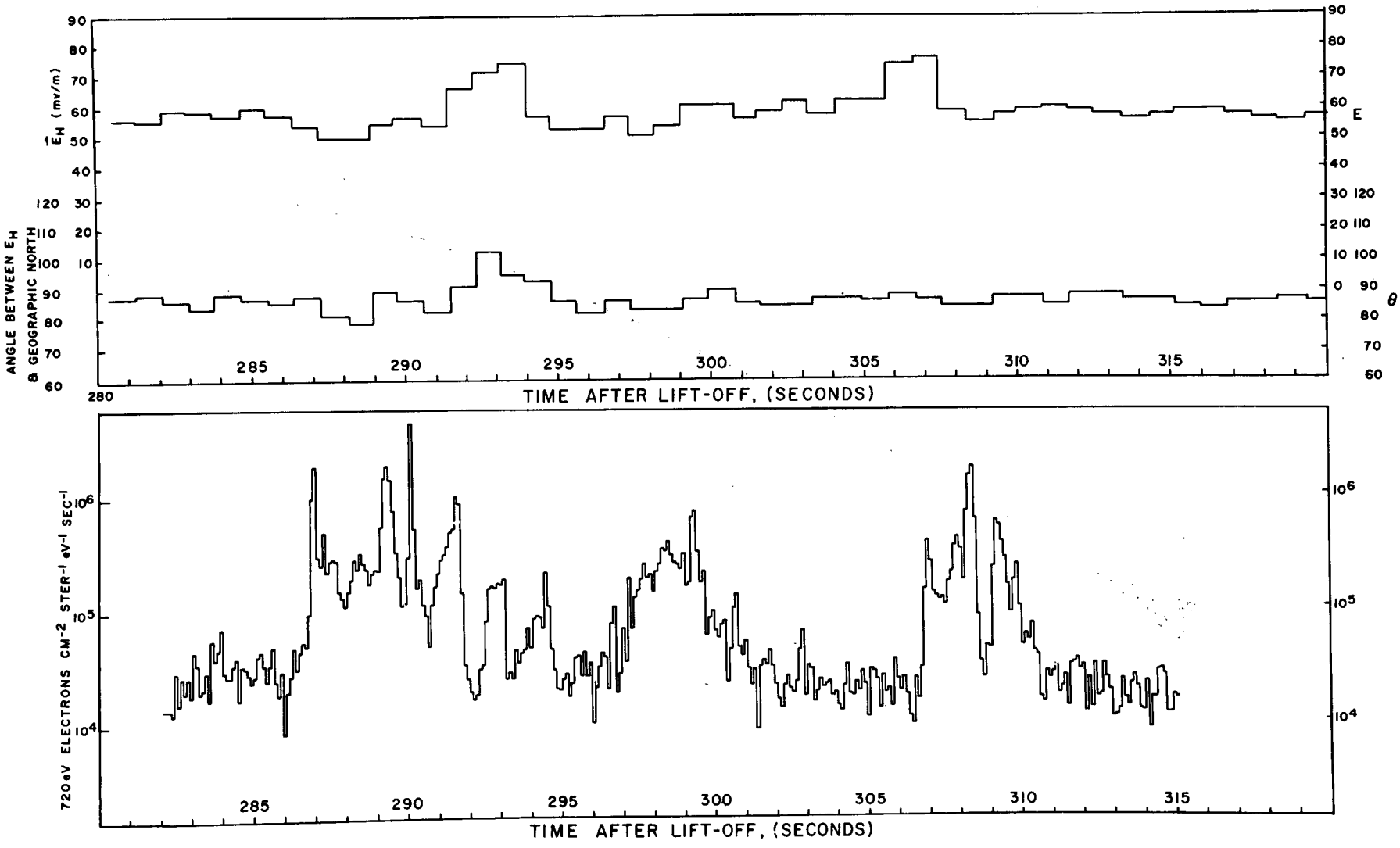
ANGLE BETWEEN E_H & GEOGRAPHIC NORTH
E_H (mv/m)
E
θ
TIME AFTER LIFT-OFF, (SECONDS)
720eV ELECTRONS CM^{-2} STER^{-1} eV^{-1} SEC^{-1}
TIME AFTER LIFT-OFF, (SECONDS)

Figure 11

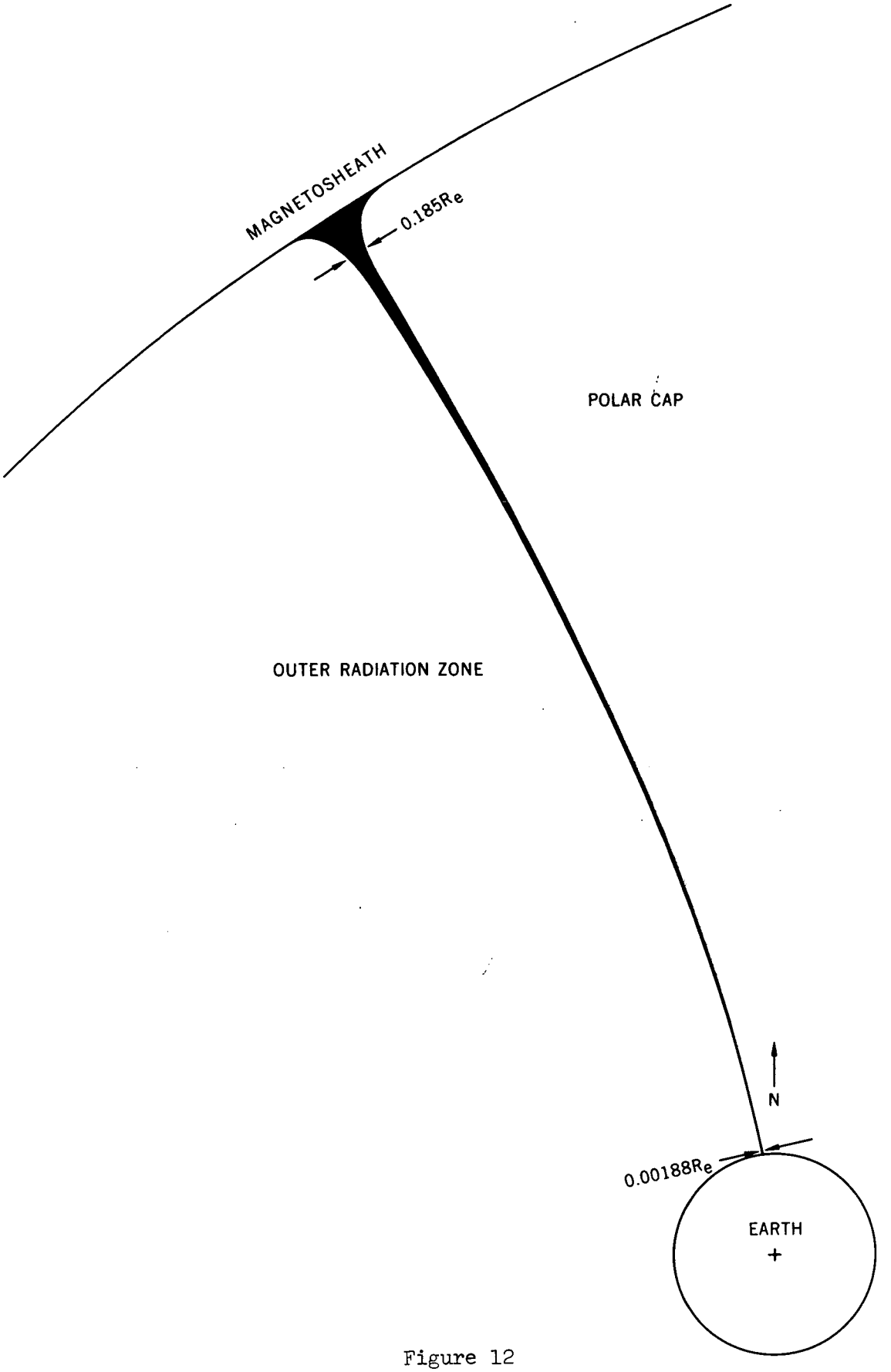

Figure 12

NASA–GSFC